3) Big Bend's Aerosol and Extinction Budgets during BRAVO

3.1 Introduction

The primary goal of the BRAVO study was to apportion the major aerosol species to their emission sources, with the secondary goals of understanding the physio/chemical/optical properties of aerosols at Big Bend and surrounding areas. To achieve the secondary goals, a number of detailed measurements of the particulate chemical composition, size distribution, hygroscopicity, and the particles' optical properties were made (see chapter 2). These measurements were sufficient to perform chemical and optical closure calculations on the measured aerosol. This chapter reports on the findings from these measurements.

Past studies have achieved closure between fine mass estimated from measured species and gravimetric mass and estimated or modeled fine particle scattering and measured scattering. However, coarse particle scattering plus absorption, as determined using open air nephelometery and filter based absorption measurements, is underestimated in routine monitoring systems by factors of as much as two [*Malm et al.*, 2000b]. To address this issue, special attention was given to measuring large particle (>1.0 μm) physio-chemical characteristics. Detailed chemical composition was measured in the fine (0.0–2.5 μm) and coarse (2.5–10.0 μm) modes (IMPROVE sampling system), as well as in eight size ranges using the MOUDI and DRUM impactors. Inorganic ions, elements, and organic and elemental carbon were measured with the IMPROVE system, inorganic ions with the MOUDI impactor, and soil related elements with a DRUM sampler. Optical measurements were made with ambient integrating nephelometers with one fitted with a cyclone (admitting particles with diameters <2.5 μm), another with PM_{10} inlet, and a third in the "open air" configuration. Fine particle absorption estimates were made with an aethalometer and from measurements of elemental carbon. The hygroscopic properties of ambient particles were examined using a humidograph with the ability to measure scattering as a function of humidity over ranges of about 15–95%. *Day et al.* [2000] described the instrument design in some detail and therefore its operation will only be summarized here.

Experiments were designed such that observables could be estimated or modeled in a number of different ways. Mass was gravimetrically determined for both D_{aero} <10 and 2.5 μm, which can be compared to reconstructed mass based on measured aerosol species. Dry and ambient scattering coefficients were measured, which in turn can be compared to modeled scattering coefficients that are based on aerosol species mass and size measurements. Humidograph measurements of scattering coefficients as functions of relative humidity can be compared to modeled scattering coefficients that include thermodynamic model predictions of inorganic aerosol hygroscopic growth.

Previous studies of aerosol hygroscopicity have been made using tandem differential mobility analyzers (TDMA) and have been summarized in *Cocker et al.* [2001]. Most studies used humidification ranges of 80–90%. A number of these studies reported two growth modes: a less hygroscopic mode with growth factors of 1.0–1.4 and more hygroscopic mode with growth factors as high as 1.8. In chamber studies, *Virkkula et al.* [1999] reported a growth factor of about 1.1 for a no-seed secondary organic case and a growth factor starting at 1.5 for an ammonium sulfate seed, but dropping to 1.1 near the end of the experiment. The affinity of organic compounds for water, particularly those organic species found in the ambient atmosphere, is not as well characterized, despite the fact these species often account for a significant amount of the total fine mass in continental aerosols [*Malm et al.,* 1994]. As reviewed

by *Saxena and Hildemann* [1996], organic particulate matter contains hundreds of compounds, spanning a range of carbon numbers, functional groups, and solubility in polar and non-polar solvents.

Measurement of particle scattering as a function of relative humidity was pioneered by *Covert et al.* [1979] and *Waggoner et al.* [1983]. They made limited measurements at a number of locations including Tyson, Missouri, Point Reyes, California, Shenandoah National Park, and Houston, Texas. *Malm and Day* [2001] reported on measurements of the relative humidity enhancement factor which is defined to be the ratio of the scattering coefficient at some relative humidity divided by the scattering coefficient at some minimum relative humidity ($f(RH)=b_{scat}(RH)/b_{scat}(RH_{min})$). Measurements were carried out at Great Smoky Mountains and Grand Canyon national parks. The f(RH) function was smoothly increasing as a function of increasing relative humidity for both data sets. However, for the most part, the f(RH) at Great Smoky Mountains began to increase at relative humidities just above 20%, while at Grand Canyon increases did not take place until approximately 40–45%, and in some cases not until 60%. At Grand Canyon, the f(RH) was more varied than at Great Smoky Mountains. For instance, in the range of 80–85% relative humidity the f(RH) values varied between 1.53 and 2.75 at Great Smoky Mountains, while at Grand Canyon the range was from near 1 to 4.0. In general, as the contributions of organics and soil dust to mass concentration increase, the increase of f(RH) with humidity decreases. Growth factors and ambient light-scattering efficiencies have previously been observed to be rather smooth functions of relative humidity [*Sloane,* 1986; *Malm et al.,* 2000a]. Measurements of f(RH) at coastal sites in Tasmania and Portugal showed qualitatively similar results in which pollution-dominated aerosols showed smoothly varying f(RH), though marine-dominated aerosols showed strongly deliquescent and more hygroscopic f(RH) [*Carrico et al*., 1998; 2000]. *Rood et al.* [1989] showed evidence for the existence of metastable aerosol in the ambient atmosphere. Differences in measurements of f(RH) between the deliquescence and crystallization branches were ~10% on average for polluted aerosols and ~20% on average for marine aerosols, though as much as 50% for individual RH scans [*Carrico et al.*, 2000].

A variety of scattering models were used in an attempt to reproduce measured f(RH) curves. At Great Smoky Mountains, both internally and externally mixed aerosol models were used assuming the measured sulfate ion was fully neutralized, assuming variable degrees of neutralization corresponding to the measured ammonium ion concentrations, and with and without accounting for sampling-period-to-sampling-period shifts in size distribution [*Malm et al.,* 2000a]. The model sensitivity to using the deliquescence and crystallization branches, as well as a curve smoothed between the deliquescence and crystallization points of D/D_o curves as a function of relative humidity for inorganic salts, was also explored. Scattering coefficient predictions as a function of relative humidity were most sensitive to the assumptions regarding sulfate ammoniation and the smoothed D/D_o growth curves. Changes in f(RH) as a function of assumptions concerning mixing were less than 10% on the average.

For the analysis of the data from Grand Canyon [*Malm and Day,* 2001], only the externally-mixed model was used; sulfate was assumed to be in the form of ammonium sulfate, and a smoothed f(RH) curve was used based on size distribution measurements made in previous studies. At Grand Canyon the assumptions of constant mass scattering efficiencies, complete sulfate ammoniation, and a constant f(RH) yielded, on the average, very reasonable results. However, on some days parts of the measured and predicted f(RH) curves varied by as much as

±20%. An ordinary least squares (OLS) regression between measured and predicted f(RH) values yielded a R^2= 0.82 with a slope of 1.02 ±0.006 when the intercept term was forced through zero. The implication is that, on the average, predicted f(RH) values were about 2% greater than measured. The results of both the Grand Canyon and Great Smoky Mountains studies suggested that organic aerosols were weakly hygroscopic or non-hygroscopic.

In this chapter, the chemical and optical properties of Big Bend's haze is examined and the influence particle size distribution, the degree of sulfate ammoniation, and chemical composition have on aerosol scattering dry and ambient scattering and as a function of relative humidity is further explored. Two equilibrium models, ISORROPIA [*Nenes et al.,* 1998] and the Aerosol Inorganics Model (AIM), [*Clegg et al.,* 1992, 1998b] are used to estimate inorganic aerosol growth.

3.2 Determination of Aerosol Types

The fine aerosol species at most continental sites can be classified into five major types: sulfates, nitrates, organics, light-absorbing carbon, and soil. Other fine species such as non-soil potassium, sea salt, and other trace elements are less important from a visibility standpoint. Details of standard methods for apportionment of measured mass to the various aerosol species are described in some detail in *Malm et al.* [1994]

An average ambient particulate organic compound was assumed to have a constant fraction of carbon by weight. Organic carbon mass concentration (OMC) was assumed to be [OMC] = 1.4[OC]. The factor of 1.4 corrects the organic carbon mass for other elements associated with an assumed average organic molecular composition [*White and Roberts,* 1977]. However, *Turpin and Lim* [2001] suggest that this factor could be as high as 2.1. The effect of varying this factor over a range of 1.4–2.1 is not considered here. Elemental carbon (EC) was also obtained.

Soil mass concentration (SOIL) was estimated by summing the elements predominantly associated with soil, plus oxygen for the common compounds (Al_2O_3, SiO_2, CaO, K_2O, FeO, Fe_2O_3, TiO_2), and applying a correction for other compounds such as MgO, Na_2O, water, and carbonate.

Aerosol species distributions were measured using an eight-stage MOUDI sampler and, on 41 of the 125 sampling days, the substrates were analyzed for the inorganic species. The 41 samples analyzed represented a variety of chemical and transport regimes. For the analyzed samples, the nitrate and sodium ions were found in the coarse mass fraction (1.0–10.0 μm), while the sulfate and ammonium ions were found, as expected, in the 0.1–1.0 μm, or fine size, range.

Because the majority of nitrate and sodium mass concentrations were in the coarse mode and the molar ratio of sodium to nitrate was about one, it will be assumed that nitrate was in the form of $NaNO_3$ and, furthermore, that sulfate was in the form of ammoniated sulfate. Ammoniated sulfate is calculated from the available ammonium and sulfate ion mass. The presence of Ca^{2+} in the coarse mode suggests that $Ca(NO_3)_2$ may also be present, although we did not consider this species in our analyses. It is noteworthy to point out that the IMPROVE and URG samplers used for measurements of the fine mode employed a cyclone inlet with a cutpoint aerodynamic diameter of 2.5 μm, which was typically near the middle of the coarse mode nitrate and sodium distributions. Concurrent number size distributions reported by *Hand*

et al. [2002] showed that, in general, the fine and coarse modes of the derived volume size distributions were also separated at about 1.0 μm aerodynamic diameter.

3.3 Summary of Optical Measurements

Table 3-1 summarizes the optical measurement in the form of mean, standard deviation, minimum, and maximum. The number of valid data points is also given. The extinction measurements, b_{ext}, were made with a transmissometer, while $b_{sp,open}$, $b_{sp,10\mu m}$ $b_{sp,2.5\mu m}$, and $b_{sp,dry}$ refer to scattering measurements made with an open air nephelometer, a nephelometer fitted with a PM_{10} inlet, a nephelometer fitted with a 2.5 μm inlet, and a nephelometer designed to operate with an inlet that dried the aerosol, respectively. The absorption measurements referred to in this table were estimated from light absorbing carbon measurements in the fine and coarse (PM_{10}–$PM_{2.5}$) mode. Note that $b_{sp,open}$, and $b_{sp,pm10}$, measurements of scattering by all particles and particles less than 10.0 μm, are within measurement uncertainty, the same implying few particles larger than 10.0 μm.

Table 3-1. Statistical summary of optical characteristics of fine and coarse particle absorption and scattering.

Variable (Mm^{-1})	Mean	Std Dev	Minimum	Maximum	*Valid*
b_{ext}	29.25	19.66	3.58	71.96	*54*
$b_{abs,2.5\mu m}$	1.32	0.62	0.36	2.51	*54*
$b_{abs,coarse}$	0.87	1.05	-1.26	3.05	*54*
$b_{sp,open}$	24.16	16.20	6.66	63.54	*54*
$b_{sp,pm10}$	25.11	17.25	6.12	65.71	*54*
$b_{sp,2.5,ambient}$	21.88	15.91	4.49	61.87	*54*
$b_{sp,2.5,dry}$	17.74	13.47	2.91	53.76	*54*
b_{ext}-$b_{sp,open}$	5.09	5.09	-3.94	16.16	*54*
$b_{sp,open}$-$b_{sp,2.5,ambient}$	2.29	1.22	0.65	8.07	*54*
$b_{sp,2.5,ambient}$-$b_{sp,2.5,dry}$	*4.14*	*3.46*	*0.58*	*17.87*	*54*

Figure 3-1 is a temporal plot of b_{ext}, ambient $b_{sp,2.5\mu m}$, and $b_{sp,coarse}$($b_{sp,open}$- $b_{sp,2.5\mu m}$). The difference between b_{ext} and $b_{sp,2.5\mu m}$ is coarse particle scattering and absorption. b_{abs} is not shown because its magnitude is about the same as $b_{sp,coarse}$ and nearly falls on top of the coarse scattering trace. From Figure 3-1, it is obvious that fine particle scattering is the largest single component of extinction and, therefore, fine particle scattering and extinction track each other very closely.

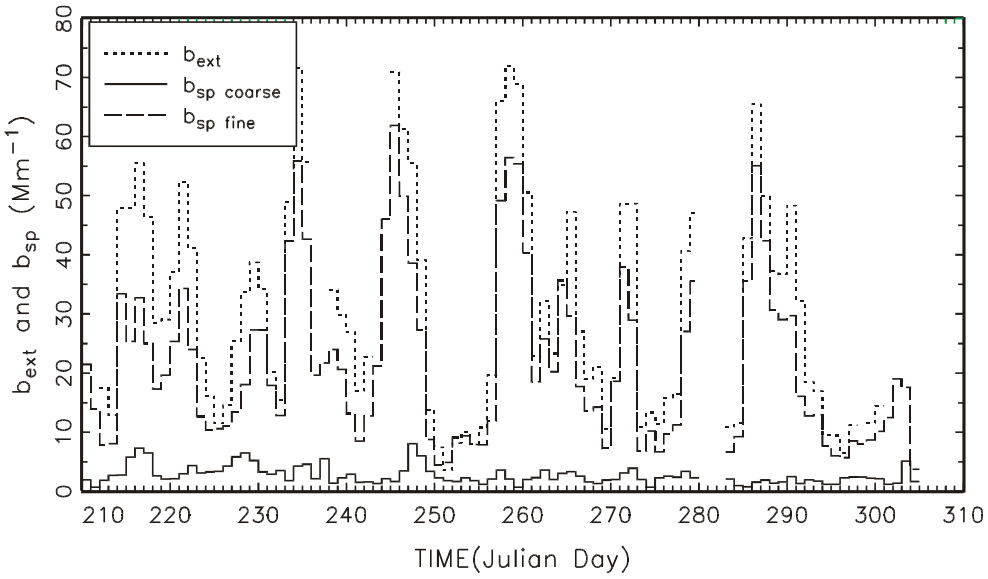

Figure 3-1. Temporal plot of b_{ext}, ambient $b_{sp,\ 2.5\mu m,}$ and $b_{sp,coarse}$.

Referencing Table 3-1, b_{ext} exceeds $b_{scat,2.5\mu m}$ by about 7.4 Mm^{-1} or 25% of aerosol extinction. Summing $b_{sp,2.5\mu m}$, $b_{sp,coarse}$, and coarse and fine absorption yields 26.38 Mm^{-1} which is 2.87 Mm^{-1}, or 10%, short of measured extinction. Coarse particle scattering is estimated to be 2.29 Mm^{-1}. Coarse particle scattering is underestimated by about a factor of one third to a half because of forward angle truncation errors and doubling coarse particle scattering would about make up for the underestimated or missing extinction [*Molenar*, 1997]. Finally, referring to Table 3-1, fine particle scattering due to water associated with hygroscopic particles ($b_{sp,2.5,ambient}$-$b_{sp,2.5,dry}$) is 4.14 Mm^{-1} or about 14% of total extinction while the total fine particle scattering fraction of extinction is 74%. Absorption, fine plus coarse, makes up another 8%. Figure 3-2 is a pie chart summarizing the fraction each of the scattering/absorption components contributes to total extinction.

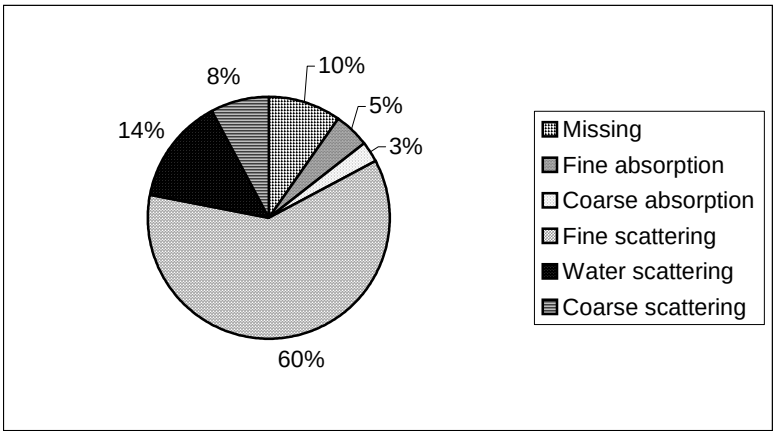

Figure 3-2. Summary of the percent scattering associated with fine and coarse particle scattering/absorption.

The degree to which absorption and/or coarse particle scattering are over- or underestimated can be explored using regression analysis. Assuming that $b_{sp,open}$-$b_{sp,2.5\mu m}$ is proportional to coarse particle scattering and b_{ext}-$b_{sp,2.5\mu m}$ is coarse particle scattering plus absorption of both coarse and fine particles, one can write the following equation:

$$(b_{ext} - b_{sp,2.5\mu m})_i = a_o + a_1(b_{sp,open} - b_{sp,2.5\mu m})_i + a_2(b_{abs,2.5\mu m} + b_{sp,course})_i \quad (3\text{-}1)$$

where i = the i^{th} sampling period and the a_o, a_1, and a_2 = constants. This series of equations can be solved using ordinary least square (OLS) regression analysis.

For purposes of the regression analysis, short temporal variability in the data was minimized by averaging to 24 hours requiring that the 24-hour data had at least 15 hours of non-missing values. The regression coefficient, a_1=2.06±0.42, is highly significant with standard error for the coefficient being about 20% while the standard error associated with total absorption, a_2=1.01±0.38, is 38%. The overall R^2 is low at only 0.23. The coefficient associated with coarse particle scattering as determined by the nephelometers ($b_{sp,open}$-$b_{sp,2.5\mu m}$) suggests that coarse particle scattering is underestimated by about a factor of two. On the other hand, the coefficient associated total absorption implies that absorption as estimated from measured fine and coarse elemental carbon is about right. Therefore this analysis suggests that the missing extinction is likely associated with an underestimate of coarse particle scattering, and fine and coarse particle extinction are, within statistical uncertainty, about right. Coarse particle absorption is 38% of total absorption.

3.4 Summary of Aerosol Species

Fine and coarse mass species concentrations are summarized in Tables 3-2 and 3-3. Measured fine mass is about 8% greater than reconstructed fine mass with ammoniated sulfate contributing 50% of the mass and organics and soil contributing 21% and 23%, respectively. The mass difference between fully neutralized or ammoniated sulfate is about 8% with ammoniated sulfate having less mass. MOUDI mass size distribution data suggested that nitrate found in the fine mode was associated with the fine tail of coarse particle sodium nitrate.

On the other hand, reconstructed coarse mass is 16% greater than gravimetric mass. Coarse mass has usually been interpreted as crustal material; however, referring to Table 3-3, 31% of reconstructed coarse mass was carbon based material while soil or crustal material made up 53% of reconstructed coarse mass. Nitrates were interpreted as sodium nitrate because MOUDI mass size distribution measurements showed very little ammonium in the coarse mode and very little sodium in the fine mode. Coarse nitrate contributed 8% of the coarse mass.

Table 3-2. Statistical summary of fine mass species concentrations. The parenthetical values are the fraction that each respective species contributes to reconstructed fine mass.

FINE MASS CONCENTRATIONS					
Variable (μg/m^3)	**Mean**	**Std Dev**	**Minimum**	**Maximum**	**Valid**
Fine Mass	6.85	4.33	0.04	19.22	116
Reconstructed FM	6.31	3.42	1.05	16.89	114
Ammoniated SO4	3.15 (0.50)	2.19	0.41	10.66	123
Sulfate Ion	2.48	1.79	0.30	8.57	123
$NaNO_3$	0.23 (0.04)	0.14	0.02	0.93	123
Nitrate Ion	0.17	0.10	0.02	0.68	123
OMC	1.34 (0.21)	0.78	0.13	5.10	116
LAC	0.15 (0.02)	0.10	0.00	0.52	116
SOIL	1.45 (0.23)	1.74	0.03	8.63	116

Table 3-3. Statistical summary of coarse mass concentrations.

COARSE MASS CONCENTRATIONS					
Variable (μg/m^3)	**Mean**	**Std Dev**	**Minimum**	**Maximum**	**Valid**
Coarse Mass	4.69	4.31	0.00	29.01	72
Reconstructed CM	5.42	4.54	0.00	32.02	72
Sulfate Ion	0.36	0.52	0.00	2.76	72
Ammoniated Sulfate	0.45 (0.08)	0.68	0.00	3.59	72
Nitrate Ion	0.30	0.26	0.00	1.32	72
$NaNO_3$	0.41 (0.08)	0.35	0.00	1.81	72
OMC	1.58 (0.29)	1.13	0.00	7.14	72
SOIL	2.90 (0.53)	3.27	0.00	23.66	72
LAC	0.09 (0.02)	0.09	0.00	0.31	72

3.5 Comparison between Measured and Modeled Dry Fine Mass Scattering Coefficients

Because little difference, on the order of 10% or less, [*Ouimette and Flagan,* 1982; *Sloane,* 1986; *Malm and Kreidenweis,* 1997; *Malm et al.,* 2000b] has been found between scattering predicted by internally and externally mixed aerosol models, the following externally mixed model was used to estimate reconstructed particle scattering:

$$b_{scat} = (e_{sf})f_s(RH)[Ammoniated\ SO_4] + (e_{nf})f_n(RH)[NaNO_3] + (e_{ocmf})f_{ocm}(RH)[OMC] + (e_{soilf})[SOIL]. \quad (3\text{-}2)$$

The brackets indicate the species concentration, while e_{sf}, e_{nf}, e_{ocmf}, and e_{soilf} refer to the fine or $PM_{2.5}$ dry mass scattering efficiencies of ammoniated sulfate, sodium nitrate, organic carbon, and soil mass concentrations, respectively, and the f(RH) term is the scattering enhancement term associated with particle growth as a function of relative humidity as obtained from the thermodynamic and Mie scattering models.

Average dry mass scattering efficiencies, e_{sf}, geometric mass mean diameters, d_g, and standard deviations, σ_g, of ammoniated sulfate were calculated using MOUDI data, corrected to physical diameter. These calculations are summarized in Table 3-4 and Figure 3-3. Figure 3-3 shows the relationship between these variables for the 41 MOUDI sample days. Some interesting relationships are readily apparent. As might be expected, as σ_g increased, e_{sf} decreased (Figure 3-3a). More interesting, at low mass levels (<2 μg/m^3) σ_g varied between about 1.4 and 2.5; however, at higher mass levels the variability in σ_g decreased (mass size distribution narrowed) and approached 1.4 at the highest mass loadings (Figure 3-3b). This narrowing of σ_g as mass levels increased was reflected in the relationship between mass and mass scattering efficiencies. Generally, as mass increased so did mass scattering efficiency (Figure 3-3c). Also, distributions with large mass mean diameters (>0.44 μm) had mass scattering efficiencies that varied from 2.5–4.0 m^2/g and σ_gs that varied between 1.4 and 2.5, while those size distributions with mass mean diameters less than about 0.28 μm had efficiencies of about 2.5m^2/g and σ_g of about 1.6 (Figures 3-3d and 3-3e). Furthermore, Figure 3-3f shows that at low mass loadings the mass mean diameter varies from 0.24–0.48 μm, while at higher mass loadings d_g varies less. These relationships were similar to those found by *Hand et al.* [2002] using measured number size distributions; however, those authors assumed that all aerosol species were internally mixed.

Table 3-4. Statistical summary of size and scattering properties of $PM_{2.5}$ ammoniated sulfate mass. The number of data points was 41.

Variable	Mean	Std Dev	Minimum	Maximum
Ammoniated Sulfate Mass ($\mu g/m^3$)	3.65	3.31	0.50	12.04
d_g (μm)	0.38	0.05	0.26	0.47
σ_g	1.88	0.26	1.50	2.42
e_{sf} (m^2/g)	3.15	0.43	2.42	4.06

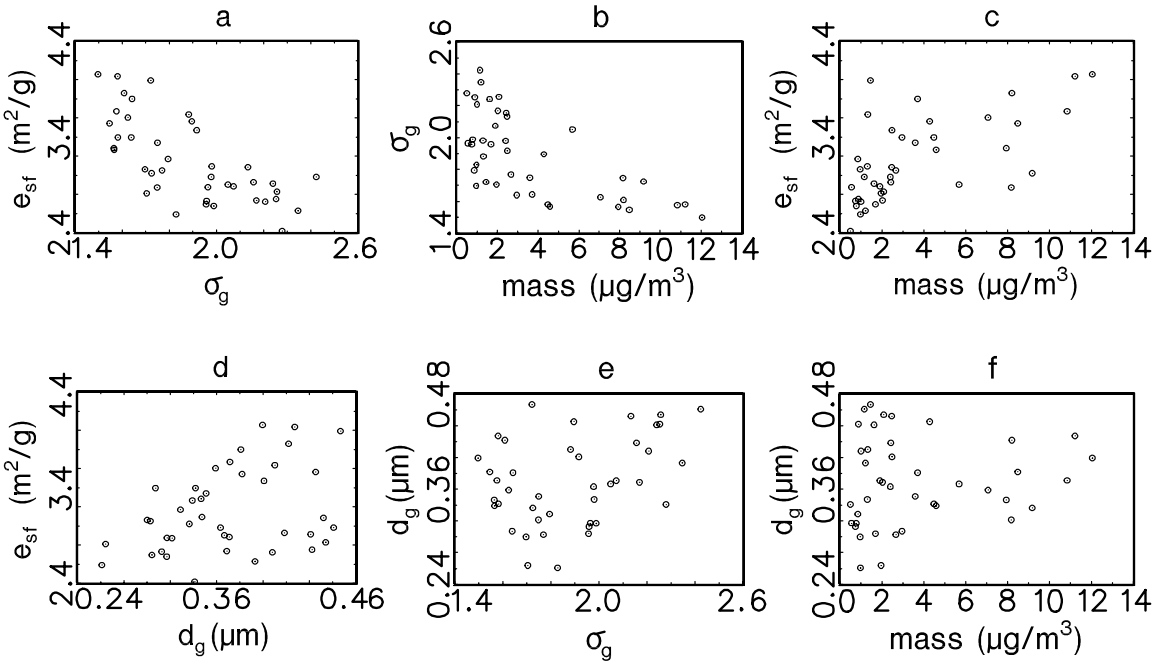

Figure 3-3. Multiple scatter plots of ammoniated sulfate dry mass scattering efficiency (eff_d), geometric mass mean diameter (d_g), geometric standard deviation (σ_g), and ammoniated sulfate mass for the 41 days on which MOUDI size mass size distribution were made.

Because mass size distribution data were only available on 41 out of 104 sampling periods, an effort was made to capture the general relationships presented in Figure 3-3 and apply them to the full dataset. To account for the daily variations in the mass scattering efficiency for ammoniated sulfate, e_{sf} was varied as a function of ammoniated sulfate mass using 2.4+0.42*[ammoniated sulfate] below ammoniated sulfate mass equal to 2.0 $\mu g/m^3$ and 3.2+0.07*[ammoniated sulfate] above 2.0 $\mu g/m^3$. Mass scattering efficiencies assumed for organics and soil were 4.0 and 1.0 m^2/g, respectively [*Trijonis et al.,* 1990; *Malm et al.,* 1994], while that used for sodium nitrate was 1.6 m^2/g. 1.6 m^2/g is an average of the 41 MOUDI samples, assuming that nitrate was in the form of sodium nitrate with its peak in the coarse fraction. The efficiency of the IMPROVE 2.5 µm cyclone inlet was used to apportion only the nitrate in particles smaller than 2.5 µm to $PM_{2.5}$ scattering.

Table 3-5 contains a summary of measured and reconstructed dry scattering coefficients along with the scattering coefficient contribution associated with each species. The difference between average measured and reconstructed dry scattering was 4%. The parenthetical values represent the fraction of scattering associated with each species. A linear regression of measured

scattering as the dependent variable and reconstructed scattering as the independent variable yielded an R^2=0.93 with a slope of 0.96±0.03 and an intercept term of 0.11±0.62. Thus we conclude that the model as given by equation 3-1 reproduced measured dry scattering quite well.

Table 3-5. Statistical summary of reconstructed and measured dry fine mass scattering and the scattering associated with each species assuming a model represented by equation 3-1. The parenthetical values are the fraction of scattering associated with each species. The number of data points was 64.

Scattering (Mm^{-1})	Mean	Std Dev	Minimum	Maximum
Reconstructed	18.45	12.49	3.56	63.17
Measured	17.73	13.30	2.27	53.76
Sulfate	12.31(0.67)	9.77	1.07	42.08
Nitrate	0.26(0.01)	0.12	0.11	0.84
Organics	5.11(0.28)	3.35	0.52	20.41
Soil	0.77(0.04)	0.96	0.06	3.73

3.6 Comparison of Equilibrium Models

To represent atmospheric aerosol water contents as functions of relative humidity, two different thermodynamic models were explored for use in this work: AIM [*Clegg et al.,* 1998b] and ISORROPIA [*Nenes et al.,* 1998]. AIM and ISORROPIA can be run in various configurations that predict the equilibrium state of the system, including partitioning of species between the liquid, solid, and gaseous phases. Here we specified the mass concentrations of aerosol-phase species based on the filter measurements described earlier, and used the models only to compute the equilibrium aerosol water contents over a range of relative humidity (RH) from 20–90%.

The version of AIM used here considers systems composed of sodium-ammonium-chloride-sulfate-nitrate-water at 298.15 K. Equilibrium states are calculated using Gibbs' energy minimization, using a global search to find the minimum. The calculations of activities of water and ions present in the aqueous phase utilize the Pitzer, Simonson, and Clegg equations [*Pitzer and Simonson*, 1986; *Clegg et al.,* 1992]. The model considers 19 possible solid phases and is valid for concentrations to saturation with respect to the solid phases. Thus, it is not generally applicable to supersaturated, metastable solutions, although the user is permitted to run in this mode, which suppresses precipitation of solids. We checked the metastable water contents against the predictions of an alternative version of AIM [*Clegg et al.,* 1998a] that is more applicable to those cases and found the differences in aerosol water content to lead to negligible differences in predicted ratios of wet to dry scattering (f(RH)) for the species considered in this report. The composition dependence of the deliquescence relative humidity is included in the formulations while the efflorescence behavior is not.

ISORROPIA considers the same chemical components as AIM, but only allows nine possible solid phases. The solution scheme differs from that used in AIM in that fifteen equilibrium reactions are solved, using a fast and stable solution algorithm [*Nenes et al.,* 1998] and permitting only certain aerosol and solution compositions depending on the ratios $R_{Na} = [Na^+]/[SO_4^{2-}]$ and $R_{SO4} = \{[Na^+]+[NH_4^+]\}/[SO_4^{2-}]$. These ratios are used to define combinations of sulfate-rich, sulfate-poor, sodium-rich, and sodium-poor domains, along with the appropriate subsets of possible solid and ionic species. This method is called "divided composition domain" [e.g., *Ansari and Pandis*, 1999]. Binary activity coefficients are calculated using the Kusik and Meissner relationships, whereas multicomponent activity coefficients are obtained from

Bromley's formula. The water content of aerosols is computed from the Zdanovskii-Stokes-Robinson (ZSR) relationship.

ISORROPIA differs from earlier equation-based models in that the mutual deliquescence relative humidity (MDRH) of mixtures of salts is considered. The value of the MDRH depends upon the mixture composition, but is always less than the minimum deliquescence humidity of any of the individual salts, so that the presence of an aqueous phase may be predicted by ISORROPIA where simpler models would predict a dry aerosol. It is important to note, however, that ISORROPIA uses data from the phase diagrams of *Potukuchi and Wexler* [1995a, 1995b] to determine the deliquescence RH (DRH); since not all possible compositions are represented, DRH behavior must be approximated from other combinations of species in such cases. The water contents in the MDRH regions are obtained by assuming a RH-weighted mean between the completely dissolved state for the most hygroscopic salt, and the completely dry state of the aerosol. This contrasts with the treatment in AIM, which solves the full minimization problem and thus can predict the gradual dissolution of solids.

ISORROPIA can also be used to compute water contents for the metastable phase. In this mode the formation of solid phases is suppressed, and calculations are made for the aqueous phase assuming the applicability of the necessary thermodynamic data at relative humidities below deliquescence. Since solid formation is not allowed for the metastable calculations, crystallization cannot be explicitly modeled. Instead, efflorescence behavior is approximated by assuming the applicability of crystallization points for ammoniated sulfate salts that are reported in the literature. Then, for calculations below these crystallization RHs, the thermodynamic data are not further extrapolated but instead a fixed, highly concentrated solution composition is assumed, leading to a discontinuity in predicted water contents that approximates the crystallization behavior.

The models were used to estimate D/D_o growth and f(RH) curves for each sampling period. For purposes of comparing these models, log normal aerosol mass size distributions were assumed for both the fine and coarse modes with geometric mass mean diameters of 0.38 and 3.0 μm, respectively, and a geometric standard deviation of 1.9 for both modes. These size parameters were derived from the average for the 41 MOUDI samples, as discussed further in the next section.

f(RH) curves were calculated for ammoniated sulfate assuming all sulfate occurred in the fine mode, while sodium nitrate was assumed to be in the coarse mode with size parameters discussed above. Because the nephelometers and fine particle samplers were operated with 2.5 μm cut points, the average mass size distribution for sodium nitrate (coarse mode) was multiplied by the sampler efficiency curve in an effort to estimate the f(RH) curves only for the fine component of the coarse mode.

Mean, maximum, and minimum differences between the metastable models are listed in Table 3-6. In about one-third of the cases, the metastable AIM f(RH) curve is well below (more than a few percent) that of ISORROPIA above the crystallization point, implying that the AIM model predicts less aerosol water than ISORROPIA. Below the crystallization point as estimated by ISORROPIA, the AIM model predicts some dissolved water and smoothly approaches zero as RH approaches zero. For a few cases the reverse was true. In general, for the metastable models, the maximum difference is always near the crystallization point with differences approaching zero for high RH values.

Table 3-6. Statistical summary of the mean percent difference between f(RH) curves in specific relative humidity ranges that were derived from aerosol growth predicted by the AIM and ISORROPIA models. The number of data points is 66.

	ISORROPIA minus AIM (metastable)		
RH	**Mean**	**Minimum**	**Maximum**
15-20	-0.06	-0.13	0.03
20-25	-0.10	-0.17	0.01
25-30	-0.14	-0.21	-0.01
30-35	-0.17	-0.25	-0.03
35-40	-0.01	-0.06	0.08
40-45	-0.01	-0.06	0.08
45-50	0.00	-0.06	0.07
50-55	0.00	-0.05	0.07
55-60	0.00	-0.04	0.06
60-65	0.01	-0.03	0.05
65-70	0.01	-0.04	0.05
70-75	0.02	-0.04	0.05
75-80	0.02	-0.03	0.05
80-85	0.03	-0.02	0.06
85-90	0.03	-0.01	0.07
90-95	0.00	-0.04	0.06

Generally, the deliquescence points predicted by the two models were the same within a few RH percentage points and, because the AIM model accounted for intermolecular interactions, the AIM model predicted deliquescence points which were less "abrupt" than ISORROPIA. Therefore, as with the metastable branch, the maximum difference between the models occurred at the deliquescence points.

3.7 Comparison of Measured and Theoretical Ambient (Wet) Fine Particle Scattering Coefficients

Table 3-7 summarizes the comparisons of measured and modeled ambient scattering coefficients as well as the contribution of each species to ambient scattering coefficients based on equation 3-1. Twenty-four hour average deliquescence and crystallization f(RH) values were calculated for ammoniated sulfate and sodium nitrate for each of the three equilibrium models described above by averaging hourly f(RH) values. As discussed above, it was assumed that all sulfate and ammonium were in the fine mode while nitrate was in the form of sodium nitrate and had a concentration peak in the coarse mode. The f(RH) of sodium nitrate was based on the fraction of this $NaNO_3$ mass in particles smaller than 2.5 μm. It was assumed that the aerosol composition and size distribution were constant over a 24-hour period, but the water contents varied hourly as a function of relative humidity. f(RH) for organics was assumed to be one, that is, they were assumed to be non-hygroscopic.

Table 3-7. Statistical summary of measured and reconstructed ambient fine mass scattering and scattering associated with each species. Ambient scattering predictions resulting from using different equilibrium model assumptions are also presented. The parenthetical values are the percent scattering associated with that species assuming the AIM metastable equilibrium model. The number of data points was 104.

Variable	Mean	Std Dev	Minimum	Maximum
RH (%)	44.63	11.68	20.92	74.38
Measured Ambient $b_{sp2.5}$ (Mm^{-1})	20.94	13.71	3.62	61.87
SOIL (Mm^{-1})	1.43(6.9)	1.78	0.06	8.63
OCM (Mm^{-1})	5.13(24.7)	3.74	0.60	26.67
Sulfate Ambient (AIM metastable) (Mm^{-1})	13.64(65.6)	10.89	1.77	52.16
Sulfate Dry (Mm^{-1})	9.11	7.49	1.02	40.13
Nitrate Ambient (AIM metastable) (Mm^{-1})	0.60(2.9)	0.38	0.14	1.99
Nitrate Dry (Mm^{-1})	0.34	0.19	0.11	0.99
Theoretical Dry $b_{sp2.5}$ (Mm^{-1})	16.01	10.66	3.24	67.47
Theoretical Ambient $b_{sp2.5}$ (AIM metastable) (Mm^{-1})	20.80	13.74	4.71	79.61
Theoretical Ambient $b_{sp2.5}$ (AIM deliquescence) (Mm^{-1})	18.33	12.58	3.68	74.05
Theoretical Ambient $b_{sp2.5}$ (ISO metastable) (Mm^{-1})	20.49	13.92	4.33	81.00

As pointed out above, ISORROPIA predicted almost no water below the crystallization point for the metastable branch, while under the "no solids" option the AIM model predicted some water below this point. Some examples of the effect that assuming water contents as given by either the crystallization or deliquescence branch had on predicted scattering are presented in Table 3-8. Average modeled dry scattering was 16.01 Mm^{-1} while average ambient scattering using the AIM metastable f(RH) curve and hourly values of relative humidity was 20.80 Mm^{-1}, which is nearly equal (1% difference) to the average measured ambient scattering value of 20.94 Mm^{-1}. Even though the AIM metastable branch ascribed some water to the aerosol below the ISORROPIA crystallization point, the average ambient scattering predicted using the ISORROPIA model was only about 1.5% less than the model using the AIM metastable solution assumptions. Using the AIM deliquescence branch yielded an ambient modeled value of 18.33 Mm^{-1} which was about 12% less than the average theoretical value using AIM metastable branch.

Table 3-8. Statistical summary of the difference between modeled and observed f(RH).

RH	Mean	Std Dev	Minimum	Maximum	N
20-25	1.37	3.33	-2.00	10.25	14
25-30	-0.48	3.03	-7.15	5.51	27
30-35	-0.51	3.42	-4.94	12.85	29
35-40	0.11	4.55	-6.64	18.07	29
40-45	-1.20	4.79	-7.78	16.87	29
45-50	-1.29	4.76	-7.97	15.28	29
50-55	-0.84	4.64	-7.04	15.50	29
55-60	-0.30	5.42	-11.36	18.02	29
60-65	0.44	3.50	-6.30	7.43	28
65-70	1.73	5.39	-10.30	16.08	29
70-75	2.32	6.03	-6.89	18.86	28

75-80	2.89	7.17	-8.19	19.98	27
80-85	3.82	10.00	-10.11	30.64	25
85-90	4.88	14.55	-12.15	43.07	20
90-95	-1.63	15.59	-17.24	36.33	15

Based on this analysis, the model using metastable water content from AIM to compute the f(RH) curves yielded the best overall fit to measured ambient scattering. An OLS estimate, with measured and theoretical ambient scattering and with the AIM metastable f(RH) curves as the dependent and independent variables, respectively, resulted in an R^2 of 0.90 with a slope of 0.99 ± 0.02. Using the ISORROPIA metastable f(RH) curves only marginally degraded the comparison between modeled and measured ambient scattering, while use of the deliquescence f(RH) curves significantly degraded the fit (>10%), implying that, in general, the ambient aerosols had been exposed to relative humidities greater than the deliquescence relative humidity and were on the crystallization branch of the curve. Despite the good agreement between predictions and measurements that was found with this approach, it is also possible that other species, namely organic carbon compounds, were responsible for the retention of water that we attribute to the metastable water associated with inorganic compounds. We explore this possibility further in the following sections.

Assuming the AIM metastable state water content and the external mixture model, sulfates and organics contributed 65.6 and 24.7 % of $PM_{2.5}$ ambient scattering while soil contributed 6.9% and nitrates 2.9%. The difference between theoretical ambient and dry $PM_{2.5}$ scattering was about 4.8 Mm^{-1} or 19%, implying that despite the study average relative humidity of only 44%, 19% of ambient scattering was associated with sulfate and nitrate water absorption. Ambient sulfate scattering was 33% greater than dry scattering while $PM_{2.5}$ nitrate scattering, which was small compared to sulfate scattering, increased by 43%. Also, 19% was close to the scattering difference measured by the ambient and dry $PM_{2.5}$ nephelometers. It should be noted that the calculations presented in Table 3-8 are for 104 sampling days while concurrent ambient and dry nephelometer scattering data were available on only 54 days.

The "best fit" model assumed only inorganic salts were hygroscopic and that their hygroscopicity was described by the AIM metastable f(RH) curve. These assumptions can be further explored by comparing measured f(RH) curves to those theoretically estimated using the model described by equation 3-1 in combination with f(RH) curves associated with various equilibrium models and the assumption concerning the hygroscopicity of carbonaceous material.

3.8 Comparison of Measured and Theoretical Scattering Coefficients as Functions of Relative Humidity

To estimate f(RH) curves, one Radiance Research nephelometer was operated continuously in a dry mode while a second nephelometer was scanned through relative humidities that ranged from about 20% to 90%. The ambient aerosol was first dried from ambient relative humidity, usually about 40%, to relative humidities less than ambient and then humidified to humidities greater than ambient. Figure 3-4 shows a typical relative humidity “scan” (Julian Day 284) with the dotted and solid lines representing the dry and relative humidity dependent nephelometers, respectively, and the inset showing the resultant f(RH) curve. The minute to minute changes in aerosol concentration as represented by the dry scattering were quite variable. In this example, during the first half of the day aerosol scattering was approximately 10 Mm^{-1}, while during the second half aerosol scattering was more variable and on the average

about 30 Mm^{-1}. During the scan the dry scattering varied between 20 and 30 Mm^{-1}. The ambient f(RH) curves were then calculated by dividing the instantaneous variable RH b_{scat} by the instantaneous dry scattering coefficient $b_{scat}(RH)/b_{scat}(RH_{min})$. Not accounting for the short term temporal variability of dry scattering would introduce significant error into the f(RH) determination.

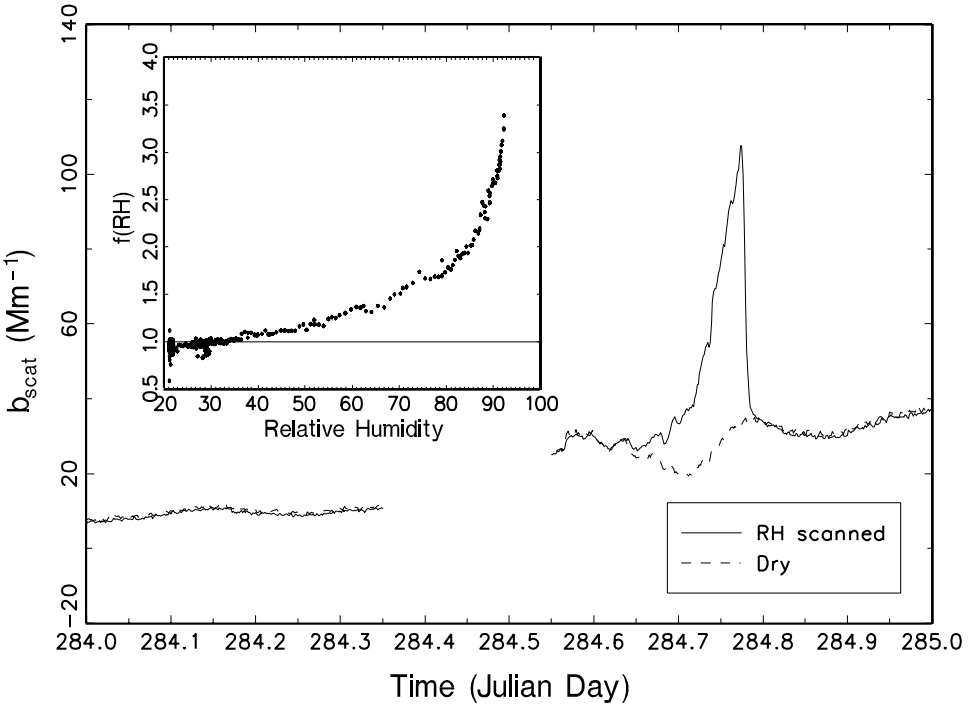

Figure 3-4. An example of dry and relative humidity ramped scattering coefficient for Julian Day 284. The hours showing missing data correspond to a calibration period.

Operating the humidograph in this configuration could have resulted in: 1) observation of crystallization if the ambient aerosol had been exposed to relative humidities above its deliquescence point and the crystallization point was below the ambient relative humidity, 2) observation of deliquescence if the aerosol had not been exposed to humidities above the deliquescence point and the ambient relative humidity was below the deliquescence point, or 3) observation of a continuous f(RH) curve over the entire RH range.

Because aerosol speciation data were collected using filter measurements that aggregated aerosol concentration into 24-hour averages, direct comparison of 24-hour theoretical f(RH) curves based on the use of equation 3-1 to measurements of f(RH) that were made on the time scale of a few hours was problematic. *Hand et al.* [2002] reported dry scattering estimates derived from dry number size distribution measurements which show that fine particle scattering and aerosol concentration track each other (R^2=0.97) on time scales on the order of minutes, suggesting that sulfate and organic mass concentrations, the primary constituents of the fine mode, varied temporally in proportion to dry scattering. Furthermore, *Hand et al*. [2002] reported a high degree of correlation between dry scattering and highly time-resolved sulfate measurements. An OLS regression between the two variables resulted in an R^2=0.86. Therefore, to account for the small time scale variation (<1 hour), the 24-hour average sulfate and organic mass concentrations were temporally scaled to the dry nephelometer data such that the sulfate

and organic scaled data integrated to the 24-hour average concentrations but reflected short-time scale fluctuations.

The dry and relative humidity scanned $PM_{2.5}$ nephelometer measurements were simulated using equation 3-1 with f(RH)=1 for organics and with the temporally adjusted sulfate and organic data on a two minute by two minute basis. Soil and nitrate mass concentrations were not adjusted for short term temporal fluctuations, and the mass scattering efficiencies applied for these species were those determined for that fraction of their masses found in the fine aerosol mode. Theoretical ambient f(RH) curves were then calculated using $b_{scat}(RH)/b_{scat}(RH_{min})$.

Forty-four f(RH) scans were made between Julian Day 238 and 301. The average measured and calculated f(RH) values are summarized in Table 3-8. Figures 3-5, 3-6, 3-7, and 3-8 show four general types of behavior of ambient and theoretical f(RH) curves. The solid line in each figure is a running three point average of two minute data while error bars are plotted every 5^{th} data point. The uncertainty associated with relative humidity is calculated from the uncertainty inherent in the RH sensor (±2%) [*Rotronic Instrument Corp*., 1998] and from the uncertainty in RH caused by a change in temperature inside the nephelometer. The exact RH inside the nephelometer is unknown; however, it is bounded by the RH at the inlet and outlet of the instrument. At low RH this difference is less than 1% (as estimated from a temperature difference of 0.3 ^{o}C), while at 90% RH the difference in RH is on the order of 2%. Therefore the combined uncertainty is on the order of ±3% at high RH values and less at lower humidities. To be conservative, the maximum uncertainty of ± 3% is presented in Figures 3-3 through 3-6. The uncertainty in f(RH) is based on a nephelometer measurement uncertainty of 5% [*Molenar,* 1997].

The dotted and dashed lines correspond to various model calculations. There were five days where there was a clear deliquescence point; one day, Julian Day 275, is shown in Figure 3-5. The model calculations shown in Figure 3-5 were based on the AIM ammoniated sulfate deliquescence growth for an ammonium to sulfate ratio of 1.74. There were two modeled deliquescence points at about 68% and 75% which correspond closely to the measured deliquescence points. On Julian Day 301 the ammonium to sulfate molar ratio was 1.8, and again the modeled and measured deliquescence points match within a few RH percentage points. However, on three other days when the ammonium to sulfate ratio was measured to be near two (fully neutralized), the model-predicted deliquescence points, as expected, were near 80% while the measured deliquescence points were at approximately 65–70% relative humidity. Undoubtedly the hygroscopic salt was not pure ammonium sulfate. On one of the three days MOUDI mass size distribution data were available and did show 1.1 and 0.22 nanomoles m^{-3} of K^+ and Ca^{++} in addition to 43.0 nanomoles m^{-3} of NH_4^+ and 22.2 nanomoles m^{-3} of SO_4^{2-}. However, neither the ISORROPIA nor AIM models incorporate K^+ or Ca^{++} in the equilibrium calculation. The average mean difference relative to the measured f(RH) curve above 80% was 17%.

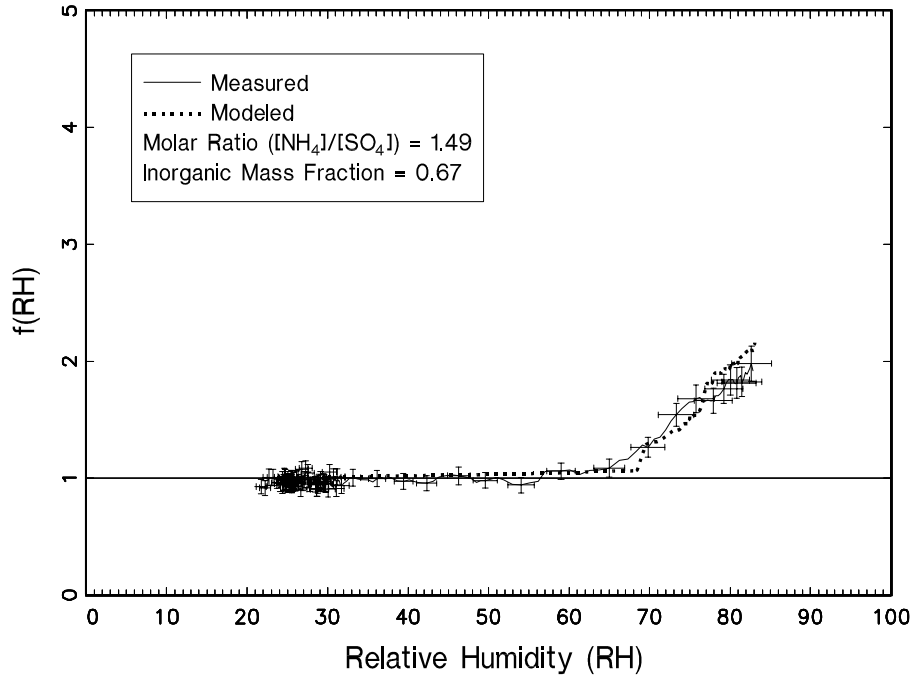

Figure 3-5. An example of measured and modeled f(RH) curves where deliquescence was observed for Julian Day 275. The molar ratio of ammonium to sulfate was 1.49 and the inorganic (SO_4+NH_4+NO_3+Na) fine mass fraction was 0.67.

Figure 3-6 shows one of five days, Julian Day 286, where there are intimations of observed crystallization. Also shown in Figure 3-6 is the modeled f(RH) curve based on the ISORROPIA metastable water absorption curve. There was close agreement between the predicted and measured f(RH) curves, and the measured and modeled crystallization points agreed well. The ISORROPIA model was used because it predicted a crystallization point, whereas the AIM model, exercised in the metastable configuration, did not. On all five days the measured and predicted crystallization points agreed to within a few RH percentage points and the f(RH) curves agreed well above the crystallization points. The average difference for the five days between measured and theoretical f(RH) curves above 35% was less than 1%.

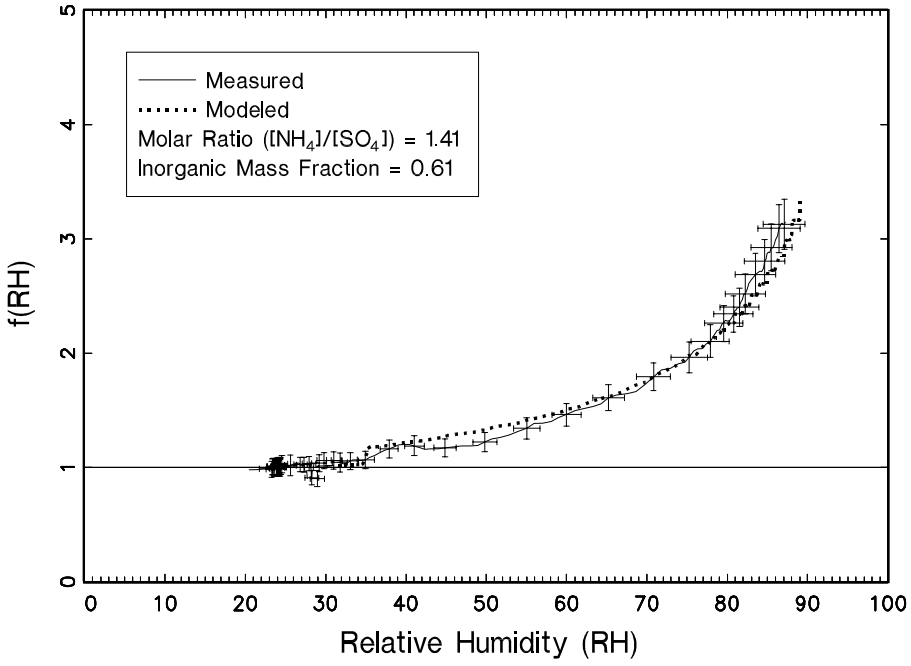

Figure 3-6. An example of measured and modeled f(RH) curves for a day where crystallization was observed. The molar ratio of ammonium to sulfate was 1.41 and the inorganic (SO_4+NH_4+NO_3+Na) fine mass fraction was 0.61.

Figure 3-7, measured on Julian Day 238, represents a third type of f(RH) curve of which there are also five cases. The measured and calculated f(RH) curves agreed well above the deliquescence point; however, below the deliquescence point the measured curve did not fall on either the ascending or descending branch of the growth curve but varied smoothly between the two points and exhibited neither deliquescence nor crystallization. On all five days water uptake began at relative humidities of about 30–35%. Above the deliquescence point (80%) the average difference between observed and modeled f(RH) for all five days was again about 1%.

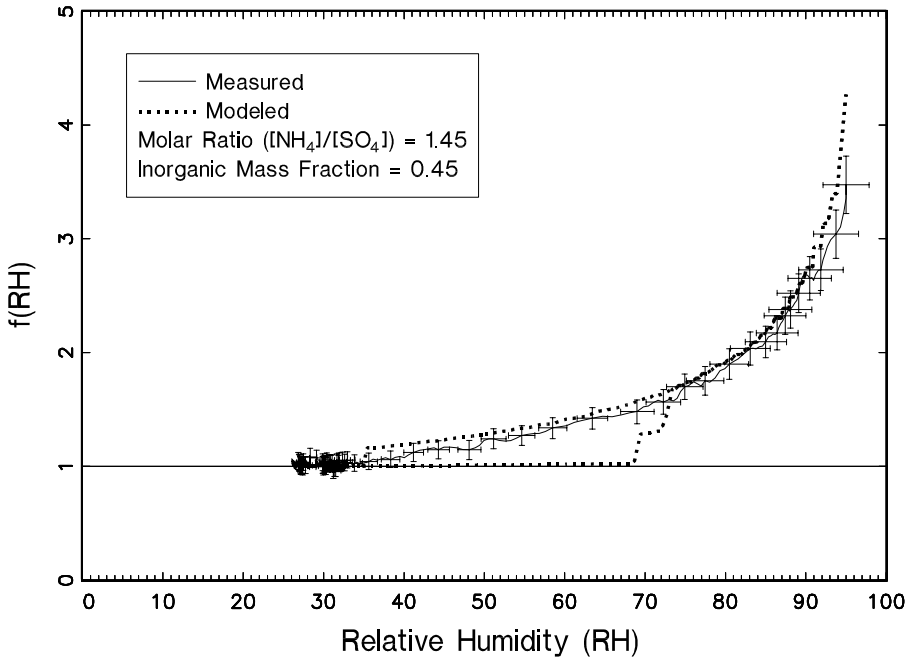

Figure 3-7. An example of a measured f(RH) curve where neither deliquescence or crystallization was observed. The modeled f(RH) curves for both deliquescence and crystallization are shown for reference. The molar ratio of ammonium to sulfate was 1.45 and the inorganic (SO_4+NH_4+NO_3+Na) fine mass fraction was 0.45.

Figure 3-8, measured on Julian Day 242, shows an example of the predominant type of f(RH) pattern of which there were 29. The 29 measured f(RH) curves again were continuous, indicating no crystallization or deliquescence from approximately one to their respective maximum values. The two theoretical f(RH) curves in Figure 3-8 are based on AIM and ISORROPIA derived metastable growth curves. The relative humidity scan for the measured f(RH) curve was initiated at a relative humidity between 26–28%, which was below the crystallization point predicted by ISORROPIA. Therefore the dry scattering coefficient based on the ISORROPIA model at 26% RH did not have any contribution due to water, while the dry scattering estimate based on AIM did. Therefore, when estimating f(RH) using $b_{scat}(RH)/b_{scat}(RH=26\%)$, the AIM based f(RH) curve was a significant fraction lower than the ISORROPIA based f(RH) curve because the AIM based $b_{scat}(RH=26\%)$ was larger than ISORROPIA. The measured and AIM based f(RH) curves were in better agreement than assuming a "dry" aerosol at 26–28%, suggesting that the aerosol was not "dried out" at the beginning of the relative humidity ramp.

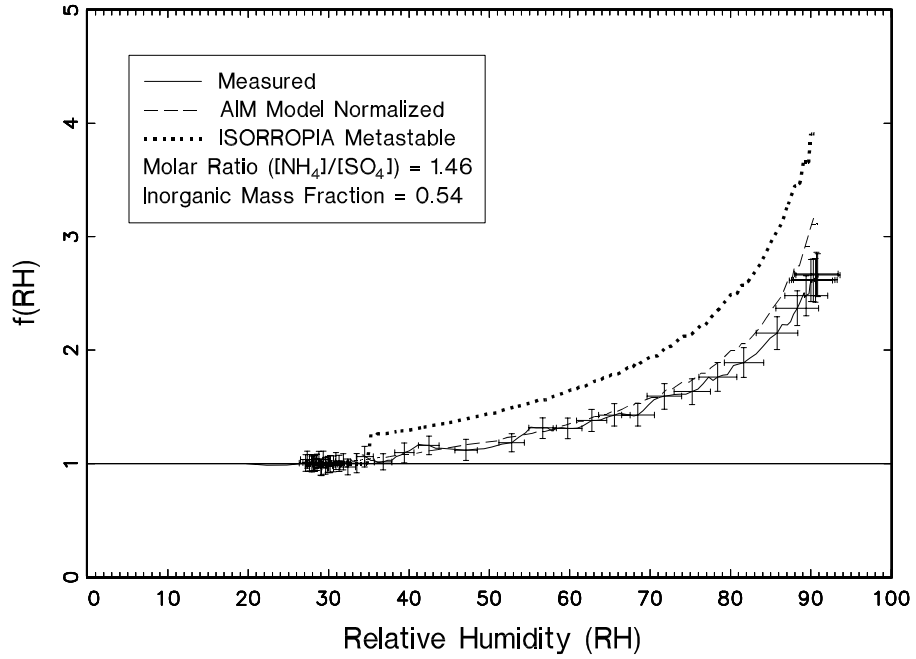

Figure 3-8. An example of measured f(RH) curve showing the over-prediction of modeled f(RH) when it was assumed the aerosol was dry below 30% RH and the modeled f(RH) when it assumed an amount of water absorption predicted by the AIM equilibrium model at 30% RH. The molar ratio of ammonium to sulfate was 1.46 and the inorganic (SO_4+NH_4+NO_3+Na) fine mass fraction was 0.54.

Table 3-8 summarizes percent differences between measured and modeled f(RH) for the 29 days in increments of 5% relative humidity. The mean difference varied from a low of -1.3% to 4.9% at 85–90% relative humidity range. The average difference above 35% relative humidity between measured and predicted f(RH) curves over all 29 days was on the order of 1%. The highest organic mass concentrations of 3.8(0.34), 5.1(0.30), and 3.2(0.27) $\mu g/m^3$ occurred on Julian Days 243, 244, and 245, respectively. The parenthetical values are the fraction of fine mass attributed to organics. The average difference, with f(RH)=1 for carbonaceous material and soil, between measured and modeled f(RH) over relative humidity ranges from 35–95% on those three days was 1.5%.

There were four days where the measured f(RH) curves were 50–60% greater than the theoretical curves at 90% relative humidity. The average difference above 80% relative humidity for the four days was 59%. Two of those days exhibited crystallization in the 35% RH range which was also predicted by the ISORROPIA model, one day showed clear deliquescence at 55% while the model predicted 65%, and one day exhibited continuous growth. All of these days were among those days with the lowest aerosol concentrations. Organics and ammoniated sulfate were less than about 1 $\mu g/m^3$ which corresponds to a dry scattering coefficient of only about 5–8 Mm^{-1}. Therefore the measured f(RH) curve reflected increased measurement uncertainty. Also, at these low concentrations, the positive organic carbon artifact was on the order of the ambient organic concentration which can result in a positive or negative bias of reported organic concentrations, depending on whether the blank correction is too large or too small. Overestimation of organic aerosol (underestimation of organic blank correction) would serve to suppress the theoretical f(RH) curve. Another possibility is that on those four days organics absorbed about as much water as the inorganic species.

3.9 Statistical Estimates of Species Specific f(RH) Curves

The amount of scattering at a specific relative humidity associated with individual species can be estimated statistically using:

$$b_{scat,water}(RH) = a_o + a_1[Ammoniated \quad SO_4] + a_2[OMC] + ... + a_n[Other\ Species] \qquad (3\text{-}3)$$

where $b_{scat,water}(RH)$ is scattering due to water at some RH, $a_1=e_s[f(RH)_s-1]$, $a_2=e_{oc}[f(RH)_{oc}-1]$, and so forth. a_o is interpreted as scattering associated with residual water or it can be set to zero, implying that all water scattering is associated with the aerosol species explicitly included in the equation. e_s and e_{oc} are the average dry mass scattering coefficients associated with sulfates and organics, respectively. $b_{scat,water}(RH)=b_{scat}(RH)-b_{scat,dry}$ is calculated on a 24-hour sampling-period-by-sampling-period basis by estimating $b_{scat}(RH)$ using measured $b_{scat}(RH)/b_{scat,dry}$ ratios and then differencing scattering at that RH and at the minimum RH. Equation 3-3 can then be solved at specific humidities using OLS regressions with or without an intercept (with or without residual water). It is emphasized that the resulting f(RH) curves are, except for the assumed dry mass scattering coefficients, based solely on measured data.

Figure 3-9 is a plot of the f(RH) curves derived from the OLS analysis without an intercept term assuming $e_s=3.2\pm0.4$ m^2/g and $e_{oc}=4.0$ m^2/g. The error bars represent the standard error of the regression coefficients, while the rectangle enclosing each error bar is associated with the standard deviation of the theoretically calculated dry mass scattering efficiencies (±0.4 m^2/g) that are based on measured sulfate size distributions.

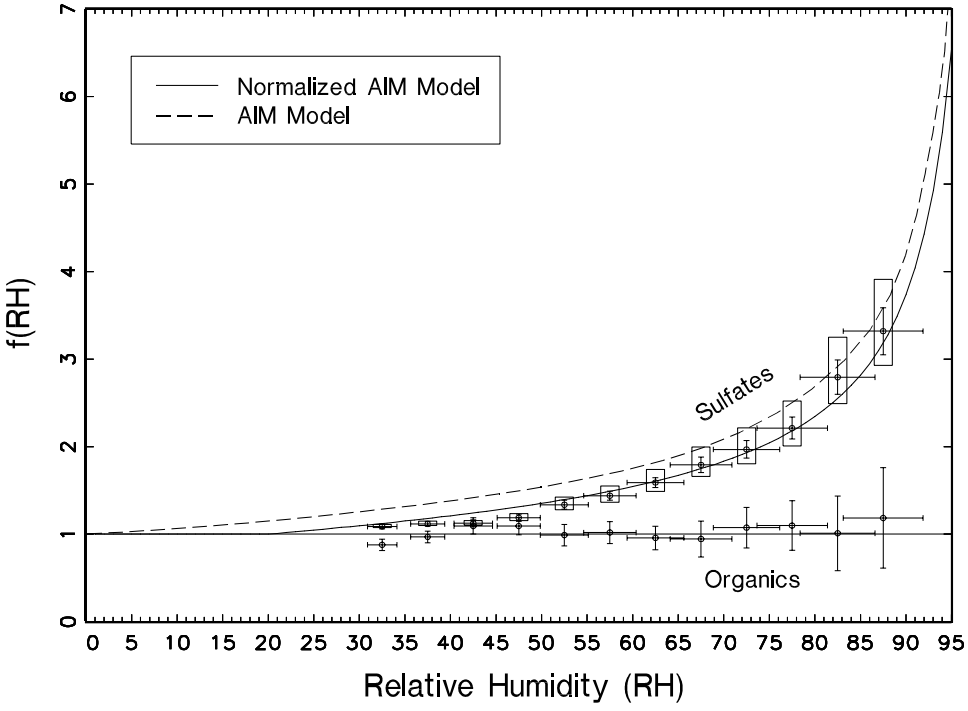

Figure 3-9. The f(RH) values for ammoniated sulfate and organics derived from a statistical model whose only inputs were measured scattering associated with absorbed water and ammoniated sulfate and organic mass concentrations. Also shown for reference are the average f(RH) curves derived from the AIM equilibrium modeled metastable D/D_0 curves without normalization and with normalization to 20% relative humidity.

The sulfate regression coefficient was significant at less than 1% at all humidities greater than 30%, while the regression coefficient associated with any other species was not statistically significant. Moreover, because the intercept term was not statistically different from zero, the results presented in Figure 3-9 were with a_o set equal to zero. The R^2 values varied between a low of 0.14 at RH=30% to above 0.80 for RH values above 50%. Even though the organic regression coefficients were not statistically significant, the implied organic f(RH) curve was included for reference. Notice that the average f(RH) data points shown in Figure 3-9 reflect some water absorption at 32% relative humidity and possible deliquescence at about 45% relative humidity and a second deliquescence point that occurred in the 75–80% range. The dotted line corresponds to the average f(RH) calculated directly from the AIM metastable growth curve while the solid line is the f(RH) normalized to 20%. The f(RH) curve, which is based on the normalized AIM metastable growth curve, approximates the statistically derived growth curve quite well.

These results are consistent with the modeled f(RH) curves where good agreement between modeled and measured f(RH) was achieved by assuming organics did not absorb water and that on most days the aerosol contained some water at relative humidities in the 20–30% range. The water retention at these low relative humidities was consistent with the amount of water predicted by the AIM equilibrium model under conditions where solids were not allowed to form (metastable state). In the statistical model no prior assumptions were made about the hygroscopicity of various aerosol species. The analysis produced an f(RH) function for ammoniated sulfate that was nearly identical to the average f(RH) curve derived from the AIM metastable growth curves that were normalized to 20% relative humidity (f(RH)normalized= f(RH)/f(20%)) and an f(RH)≈1 for organics and soil).

3.10 Summary of Particle Scattering and Absorption Estimates

The following equation is used to estimate reconstructed particle extinction:

$$\begin{aligned} b_{ext} = {} & (e_{sf})f_s(RH)[Ammoniated\ SO_4] + (e_{nf})f_n(RH)[NaNO_3] \\ & + (e_{ocmf})[OMC] + (e_{soilf})[SOIL] \\ & (e_{sc})f_s(RH)[Ammoniated\ SO_4] + (e_{nc})f_n(RH)[naNO_3] \\ & + (e_{ocmc})[OMC] + (e_{soilc})[SOIL] + 10[lacf + lacc]. \end{aligned} \tag{3-4}$$

The brackets indicate the species concentration, while e_{sf}, e_{nf}, e_{ocmf}, and e_{soilf} refer to the dry mass scattering efficiencies of ammoniated sulfate, ammonium nitrate, organic mass, and soil mass concentrations, respectively. The second set of these same variables refers to coarse mass efficiencies. $f_s(RH)$ and $f_n(RH)$ refer to the enhancement factors for sulfates and nitrates, respectively. The f(RH) curves for sulfates and nitrates were calculated using AIM derived growth curves while the f(RH) for organics was assumed to be one.

The fine and coarse scattering/absorption values are summarized in Table 3-9. The first and second rows are the average measured and reconstructed total particle extinction. The following four rows are measured and estimated coarse and fine particle scattering while remaining rows are the scattering associated with each fine and coarse species and total absorption (fine + coarse). The parenthetical values are the fraction of total particle extinction associated with the respective species. The estimated or modeled extinction is within 3% of measured while estimated coarse and fine particle scattering are within 12% and 2% of measured coarse and fine particle scattering. Coarse and fine particle scattering contribute 4.4 Mm^{-1} and

22.4 Mm^{-1}, or about 15% and 77%, respectively, to extinction while coarse plus fine particle absorption adds another 2.5 Mm^{-1} or 9%. The fractional contribution of fine plus coarse particle sulfates, nitrates, organics, and crustal material is 58.0%, 2.6%, 24.9%, and 7.3%, respectively. 8.6% of total extinction is linked to absorption with 38% associated with the coarse mode leaving 62% of absorption linked to the fine mode.

Table 3-9. Statistical summary of extinction and the contribution of each species to extinction. The parenthetical values are the fraction that each species contributes to extinction.

Variable (Mm^{-1})	Mean	Std Dev	Minimum	Maximum	Valid
b_{ext}	30.26	20.11	3.58	71.96	60
Reconstructed b_{ext}	29.31	18.58	7.46	83.95	60
$b_{sp,coarse}$	4.99	5.14	-4.78	17.65	60
Reconstructed $b_{sp,coarse}$	4.37 (14.9)	2.74	0.00	16.29	60
$b_{sp,2.5\mu m}$	22.75	16.31	4.49	61.87	60
Reconstructed $b_{sp,2.5\mu m}$	22.41 (76.5)	16.60	5.05	75.20	60
SO_4 $b_{sp,coarse}$	0.69 (2.4)	1.36	0.00	7.33	60
NO_3 $b_{sp,coarse}$	0.38 (1.3)	0.35	0.00	1.98	60
OCM $b_{sp,coarse}$	1.82 (6.2)	1.02	0.00	4.17	60
Soil $b_{sp,coarse}$	1.48 (5.1)	1.13	0.00	5.40	60
SO_4 $b_{sp,2.5\mu m}$	16.29 (55.6)	14.17	2.44	54.51	60
NO_3 $b_{sp,2.5\mu m}$	0.37 (1.3)	0.20	0.12	1.30	60
OCM $b_{sp,2.5\mu m}$	5.11 (17.4)	3.26	0.52	20.41	60
SOIL $b_{sp,2.5\mu m}$	0.64 (2.2)	0.78	0.06	3.62	60
Fine + Coarse b_{abs}	2.52 (8.6)	1.41	0.64	6.51	60

It is interesting to point out that even though crustal material makes 54% of the coarse mass on a scattering basis, it contributes less to extinction than coarse organics because organics have a mass scattering efficiency which is twice that of crustal material.

3.11 Temporal Variation in the Particulate and Light Extinction Budgets

The previous discussion examined the particulate chemical composition and contribution to light extinction averaged over the BRAVO time period. It is also instructive to examine their temporal variability. The daily fine mass species used to generate Table 3-2 are plotted in Figure 3-10. Figure 3-11 presents the daily ambient light extinction budgets during the BRAVO period.

The light extinction budgets require having valid contributions from all of the major fine and coarse aerosol measurements. However, only 60 out of 123 days had all of the necessary data (Table 3-9). The loss of more than half of the days was primarily due to missing coarse particle data. To fill in these missing days, coarse scattering was estimated using several methods. If all extinction, scattering, and absorption measurements were available, then coarse extinction was estimated by: $b_{ext,coarse} = b_{ext} - b_{sp,2.5\mu m} - b_{abs,2.5\ \mu m}$. $b_{abs,2.5\ \mu m}$ was estimated by multiplying the fine light absorbing carbon concentration by an absorption factor of 10 m^2/g. Coarse extinction was estimated this way for 78% (96/123) of the BRAVO study days. When any of these measurements were missing, coarse extinction was reconstructed from the coarse particle measurements by summing the scattering due to coarse sulfates, nitrates, soil, and organic and coarse light absorbing carbon. This method was used for 10% (12/123) of the coarse extinction values. Occasionally, total coarse mass was available, but some of the individual species concentrations, usually carbons or ions, were missing. In those cases, coarse extinction

was estimated by $b_{ext,coarse}$ = 0.6 m^2/g [Coarse mass] * (1.1), where 0.6 m^2/g is the estimated scattering efficiency of coarse mass and 1.1 is a factor to account for the additional light extinction due to coarse absorption. The 1.1 factor is the median of the coarse extinction divided by the coarse scattering for days when those values were available. This method was used for 5% (6/125) of the values. The remaining days were filled in by combining the available light scattering and absorption measurement and aerosol data and ratios of the missing and available components from the previous day.

As shown in Figure 3-10, there is a distinct difference in the chemical composition of the fine mass in the first and second half of the BRAVO study. From July 1–August 15, the fine mass is primarily composed of ammonium sulfate (35%), soil (35%), and organics (20%). In the second half of the study, post-August 15, the fine mass is primarily composed of sulfate (60%) and organics (20%) with soil comprising only 15%. In both time periods of the study, sulfate was the largest contributor to b_{ext}, accounting for 35% of the particulate b_{ext} in the first half of the study and 50% in the second half (Figure 3-11). Organic carbon accounted for 20% and 18%, and coarse mass accounted for about 30% and 20% of the particulate light extinction in the first and second half of the BRAVO study, respectively. On the haziest 1/5th of the days sulfate compounds accounted for about 55% of the particulate b_{ext} and organics about 15%. The lower contribution of organics and the fact that they have a potentially large contribution from smoke and other natural sources [*Collet et al.*, 2001; *Brown et al.*, 2002] lead us to concentrate on understanding the source attribution of sulfate.

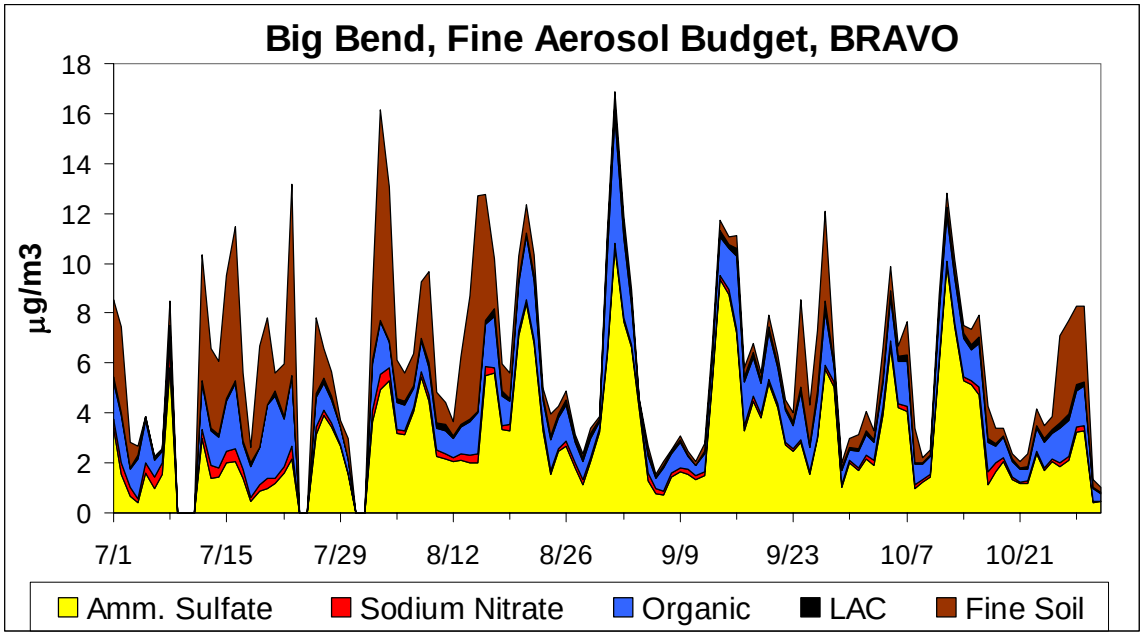

Figure 3-10. Big Bend's daily fine particulate mass budget during the BRAVO study.

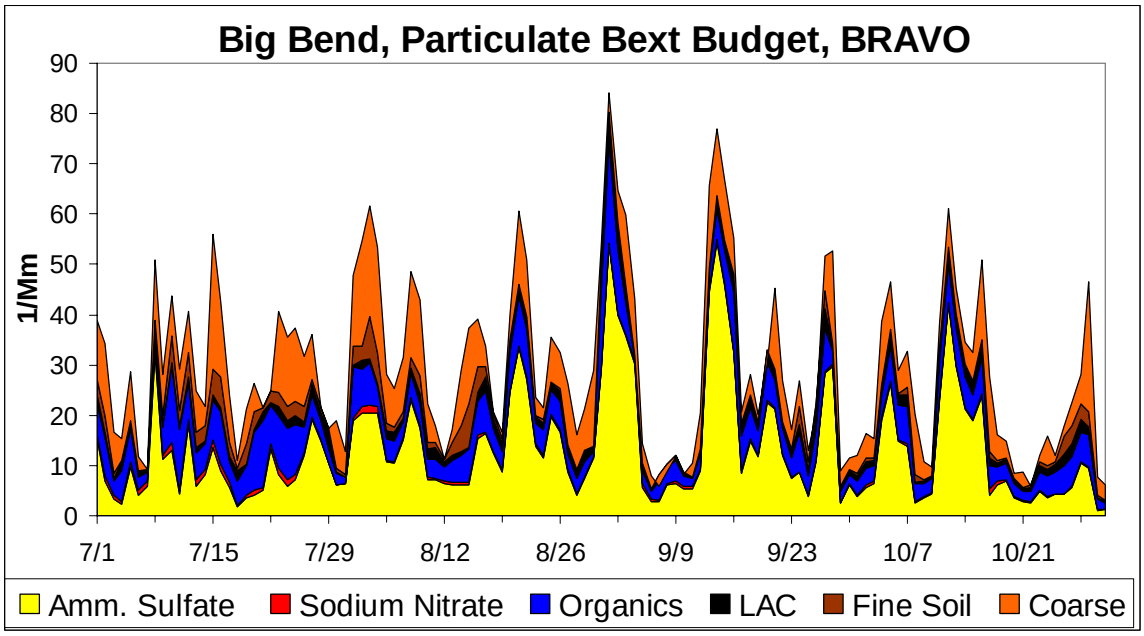

Figure 3-11. Big Bend's particulate light extinction budget during BRAVO.

3.11.1 Big Bend's Average Seasonal Light Extinction Budget

The BRAVO period can be put into a larger climatological context by examining Big Bend's extinction budget over a long time period. Figure 3-12 shows the five-year (1998 through 2002) light extinction budget from measurements made every three days at Big Bend National Park in the IMPROVE monitoring network. The contribution to b_{ext} of each particulate component was calculated based upon the regional haze guidance document [*U.S. Environmental Protection Agency*, 2003a], but the increase in scattering due to particle growth from water, i.e., f(RH), was estimated using the measured relative humidity at Big Bend.

In general, there are two periods of high haze at Big Bend National Park, one in spring when particulate sulfate and carbonaceous compounds contribute in similar amounts to haze, and another in late-summer/fall when particulate sulfate compounds are the largest contributors to haze. Similar to the BRAVO period, the particulate sulfate compounds generally contribute more to haze than any other individual aerosol component. Carbonaceous particulate matter—organic compounds and light absorbing carbon (LAC)—generally constitute the second largest individual aerosol component contributing to haze at Big Bend NP. Information from other studies shows that during late spring episodes, concentrations of carbonaceous compounds are increased due to biomass burning in Mexico and Central America. Dust, represented by a combination of fine soil and coarse mass, contributes as much to haze as particulate sulfate compounds during the months of March and April.

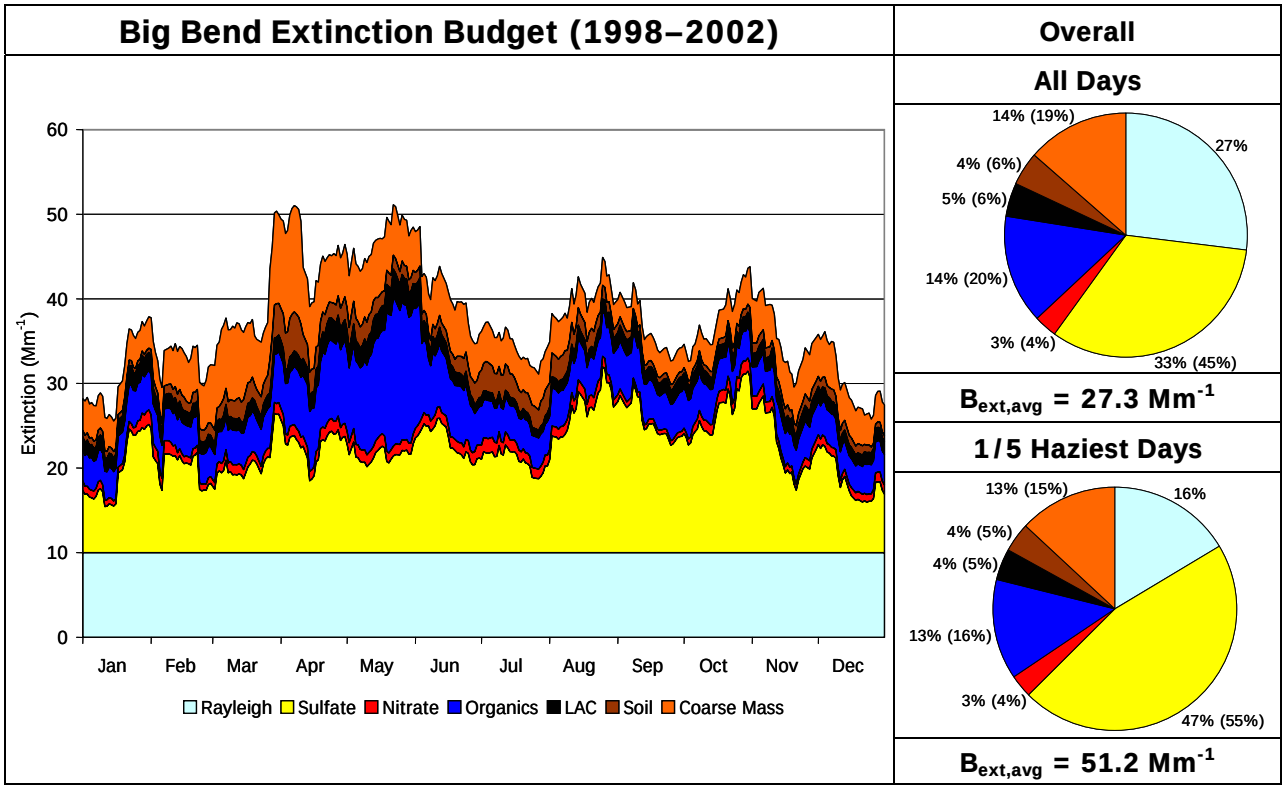

Figure 3-12. Big Bend National Park five-year light extinction budget. All days that fall on the same day of the year were averaged together, then the data were smoothed using a 15-day moving average.

Figure 3-13 contains pie diagrams that show the average estimated contributions to light extinction by the various aerosol components and Rayleigh scattering. Separate pie diagrams display the averages by calendar quarter for all days and the 1/5 haziest days each year for the five-year period from 1998 to 2002. The Rayleigh scattering percent contribution necessarily decreases for the haziest days compared to all days because its absolute contribution is taken to be constant for all days. As shown, more of the annual haziest days are in the second and third calendar quarters (63%) than in the other quarters. Particulate sulfate compounds contribute more to light extinction on the haziest days than for average days during all quarters. Over the entire five-year period the contribution to particulate light extinction increases from 45% on all days to 55% for the 1/5 haziest days (Figure 3-12).

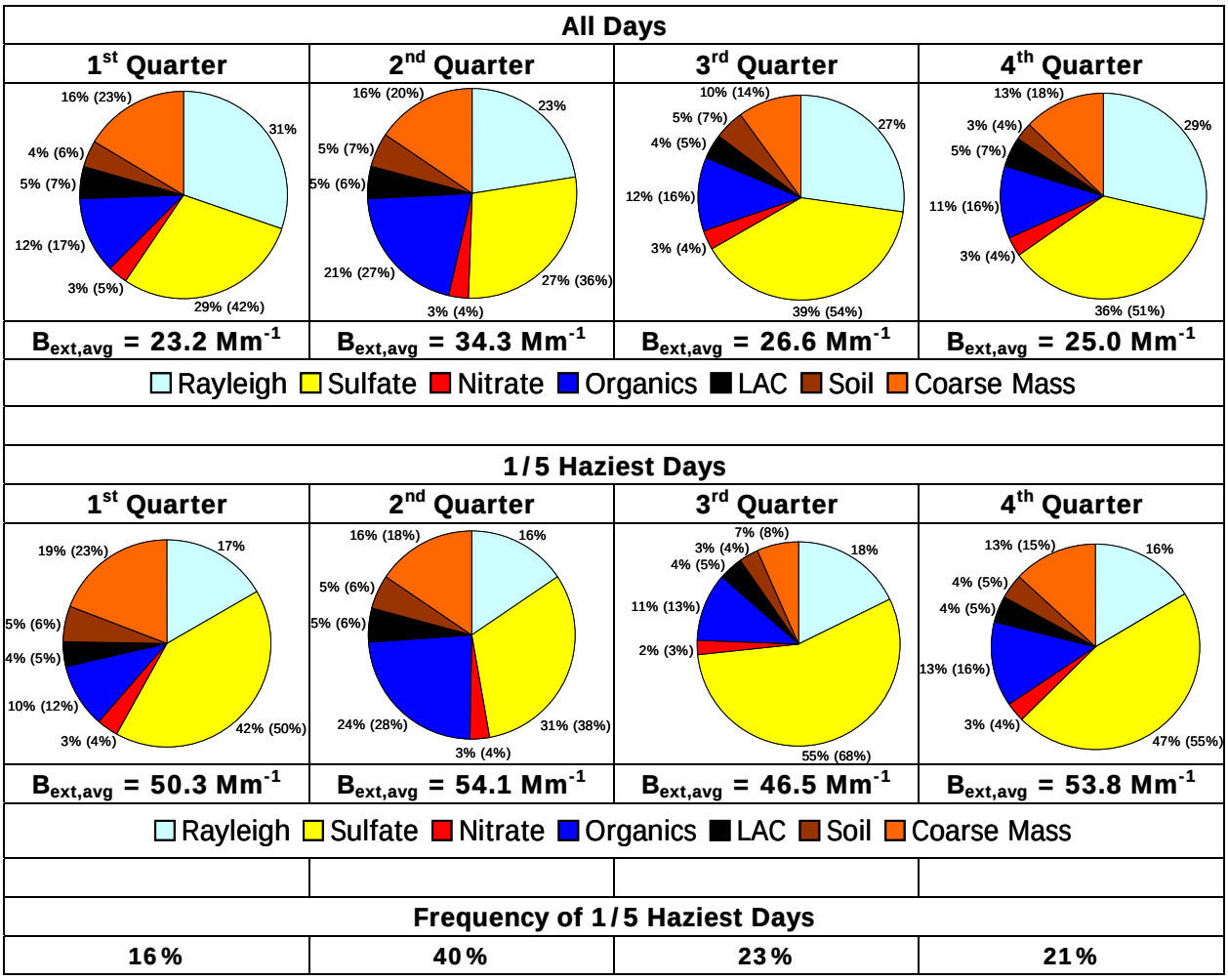

Figure 3-13. Quarterly aerosol contributions to light extinction averaged over five years (1998–2002). Top graphs: all days in each quarter; bottom graphs: annual haziest 1/5 of the days. Percent contributions to particulate haze (the non-Rayleigh light extinction) are shown in parentheses.

The contribution of carbonaceous (i.e., organic and light absorbing carbon) compounds to light extinction decreases from 26% on average to 21% on the haziest days. In the quarter with the greatest number of haziest days (2nd quarter), the contribution to particulate light extinction by carbonaceous compounds is about 34% on average and for the haziest days, which is similar to the contribution by the sulfate compounds at 36–38%.

The coarse mass is also a major contributor to the particulate light extinction accounting for 18–23% on all days and the haziest days during quarters 1 and 2. The contribution of coarse material to light extinction is similar for all days in a quarter and the haziest days, except for quarter 3 where coarse mass accounted for only 8% of the particulate light extinction on the haziest days compared to 14% on average. In the past, the coarse mass was assumed to be composed of primarily soil; however, during BRAVO soil accounted for 53% of the coarse mass, carbonaceous compounds accounted for 31%, and sulfate accounted for 8% (Table 3.3). The coarse carbon material could still be part of the wind blown dust.